Journal for ImmunoTherapy of Cancer

Spontaneous tumor regression following COVID-19 vaccination

Luana Guimaraes de Sousa ,[1] Daniel J McGrail,[2] Kaiyi Li,[1] Mario L Marques-Piubelli,[3] Cipriano Gonzalez,[1] Hui Dai,[2] Sammy Ferri-Borgogno,[4] Myrna Godoy,[5] Jared Burks ,[6] Shiaw-Yih Lin,[2] Diana Bell,[7] Renata Ferrarotto[1]

To cite: Sousa LG, McGrail DJ, Li K, *et al*. Spontaneous tumor regression following COVID-19 vaccination. *Journal for ImmunoTherapy of Cancer* 2022;**10**:e004371. doi:10.1136/jitc-2021-004371

► Additional supplemental material is published online only. To view, please visit the journal online (http://dx.doi.org/10.1136/jitc-2021-004371).

LGdS and DJM contributed equally.

Accepted 30 January 2022

For numbered affiliations see end of article.

Correspondence to
Dr Renata Ferrarotto;
RFerrarotto@mdanderson.org

ABSTRACT

Vaccination against COVID-19 is critical for immunocompromised individuals, including patients with cancer. Systemic reactogenicity, a manifestation of the innate immune response to vaccines, occurs in up to 69% of patients following vaccination with RNA-based COVID-19 vaccines. Tumor regression can occur following an intense immune-inflammatory response and novel strategies to treat cancer rely on manipulating the host immune system. Here, we report spontaneous regression of metastatic salivary gland myoepithelial carcinoma in a patient who experienced grade 3 systemic reactogenicity, following vaccination with the mRNA-1273 COVID-19 vaccine. Histological and immunophenotypic inspection of the postvaccination lung biopsy specimens showed a massive inflammatory infiltrate with scant embedded tumor clusters (<5%). Highly multiplexed imaging mass cytometry showed that the postvaccination lung metastasis samples had remarkable immune cell infiltration, including CD4+ T cells, CD8+ T cells, natural killer cells, B cells, and dendritic cells, which contrasted with very low levels of these cells in the prevaccination primary tumor and lung metastasis samples. CT scans obtained 3, 6, and 9 months after the second vaccine dose demonstrated persistent tumor shrinkage (50%, 67%, and 73% reduction, respectively), suggesting that vaccination stimulated anticancer immunity. **Insight:** This case suggests that the mRNA-1273 COVID-19 vaccine stimulated anticancer immunity and tumor regression.

INTRODUCTION

Vaccines against COVID-19 are a promising approach to prevent and mitigate COVID-19. Overall, systemic reactogenicity events have been reported by 50% and 69% of patients after the first and second doses of RNA-based COVID-19 vaccines, respectively.[1] These events, such as fever, headache, myalgias, and chills, are direct manifestations of the innate immune response to vaccination that results in the production and release of pyrogenic cytokines and inflammatory mediators, activation of complement, and recruitment of immune cells.[2]

Interestingly, spontaneous tumor regression following an intense immune-inflammatory response, usually triggered by a pathogen infection, has been recognized for centuries and guided the first steps toward immunomodulation of the microenvironment to treat cancer. The first reported immunotherapy against cancer was the inoculation of streptococcal organism into patients with unresectable sarcomas,[3] and for over three decades, administration of the BCG vaccine to promote local inflammation has been used to treat non-muscle-invasive bladder cancer.

Here, we describe dramatic tumor regression in a patient with metastatic myoepithelial carcinoma of the parotid who experienced intense reactogenicity following the second dose of the mRNA-1273 COVID-19 vaccine.

CASE REPORT

In March 2020, a 61-year-old woman was diagnosed with a T2N0MX (AJCC cancer staging manual, 8th edition) myoepithelial carcinoma of the left parotid. She underwent left parotidectomy and postoperative radiotherapy (60 Gy) to the left neck and tumor bed. CT scans performed in July 2020, after treatment completion, revealed increase in size of bilateral pulmonary nodules suggestive of metastasis (figure 1A). A CT-guided biopsy of a lung lesion confirmed metastatic disease. Given the absence of curative-intent treatment for the metastatic disease, lack of standard systemic therapy for myoepithelial carcinoma, low disease burden, and lack of symptoms, the decision was made to proceed with close surveillance.

In January 2021, approximately 10 months after the initial diagnosis of myoepithelial carcinoma, the patient received the first dose of mRNA-1273 COVID-19 vaccine. Adverse events reported were mild injection-site pain on day 1 and mild fatigue on day 2.

In February 2021, a surveillance CT scan of the chest showed a significant increase in the size of the pulmonary nodules compared with their size on the previous CT scan (figure 1B,C), obtained in November 2020.

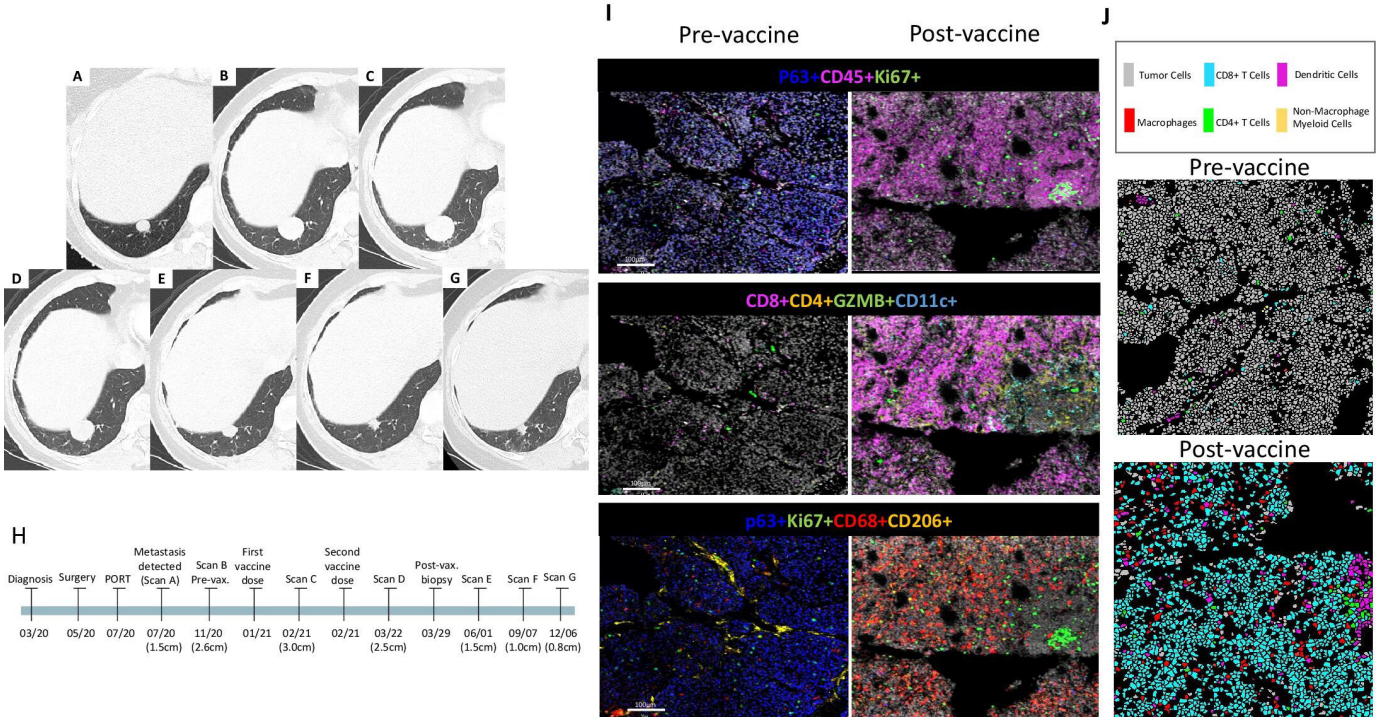

Figure 1 Temporal overview of a metastatic nodule in right lower lobe at different timepoints, before and after COVID-19 vaccination with mRNA-1273. Other bilateral pulmonary metastases (not shown) have presented the same behavior overtime. (A) In July 2020, when metastasis was initially confirmed by biopsy, the nodule measured 1.4 cm. (B) In November 2020, the nodule measured 2.6 cm. (C) In February 2021, a few days after the patient received the first dose of the mRNA-1273 vaccine, the nodule measured 3.0 cm. (D) In March 2021, 1 month after the patient received the second dose of the mRNA-1273 vaccine, the nodule measured 2.5 cm. CT images acquired approximately 3 months (E), 6 months (F), and 9 months (G) after vaccination, show progressive decrease in size of the lesion, measuring 1.5 cm, 1.0 cm, and 0.8 cm, respectively. (H) The timeline at the bottom of the figure shows the timing of events. (I) Representative images demonstrating changes in tumor immune microenvironment composition of the primary parotid tumor (pre vaccine) and the lung metastasis (post vaccine; lung-met II) using imaging mass cytometry (750×750 pixels, length×width, respectively). (J) Imaging mass cytometry cell subpopulation clusters. PORT, postoperative radiation therapy; vax., vaccination.

The decision was made to start systemic therapy in a clinical trial.

Later in February 2021, before systemic therapy was initiated, the patient received the second dose of the COVID-19 vaccine. Reported side effects were more severe than after the first dose: the patient reported a fever of 38.3°C and chills that started approximately 9 hours after vaccine administration and lasted for 2 hours. The patient also reported grade 3 fatigue, grade 2 myalgias, grade 2 muscle weakness, grade 2 headache, and mental fogginess; these symptoms persisted for 7 days after vaccination and then subside over an additional 7 days.[4]

Intriguingly, in March 2021, a CT scan of the chest revealed 13% shrinkage of the pulmonary nodules (figure 1D). Therefore, the decision was made to not proceed with the clinical trial treatment, which had been scheduled to start the day after the CT. A biopsy of a pulmonary nodule was performed at this point. Reverse transcription PCR tests for COVID-19 were performed prior to the CT of the chest and prior to the lung biopsy, both negative for COVID-19 infection.

Persistent tumor shrinkage was demonstrated on follow-up CT scans: 50%, 67%, and 73% reduction (figure 1E–G) at 3, 6, and 9 months, respectively, after the second dose of the vaccine. A timeline summarizing these events is shown in figure 1H. Therefore, we hypothesized that the tumor shrinkage was attributed to a systemic inflammatory response induced by the COVID-19 vaccine.

METHODS

The patient gave written informed consent for analysis of tumor specimens and publication of this report. All CT scans were reviewed by the same thoracic radiologist. Details of tumor molecular profiling, including immunohistochemical analysis, targeted-exome sequencing, and imaging mass cytometry, are provided in the online supplemental.

RESULTS

Molecular profiling and immunohistochemistry suggest a poorly immunogenic tumor

Molecular profiling performed with next-generation sequencing of the primary tumor sample revealed pathogenic somatic mutations in *NOTCH3* and *TP53* (online supplemental). The tumor was microsatellite stable and mutational burden was low (≤5 mutations/

megabase). Histological analysis of H&E-stained sections revealed both primary tumor and lung metastasis prior to COVID-19 vaccination had rare and scattered immune cells restricted to the tumor border (online supplemental figure 1). Consistently, immunohistochemistry showed negative staining for PD-L1 (antibody clone 22C3).

Imaging mass cytometry reveals robust tumor immune cell infiltration following the second dose of mRNA-1273 vaccine

On histological and immunophenotypic inspection of the tumor samples, a massive inflammatory infiltrate with scant tumor clusters (<5%) embedded in was observed in the postvaccination lung biopsy specimen (online supplemental figure 1), suggesting that the tumor regression was associated with induction of an anticancer immune response.

To comprehensively profile the tumor immune microenvironment (TIME), we performed highly multiplexed imaging mass cytometry on representative prevaccination (primary tumor and lung metastasis) and postvaccination (lung metastasis) samples (figure 1I–J). Notably, the postvaccination lung metastasis samples had remarkable immune cell infiltration, including infiltration by CD4+ T cells, CD8+ T cells, natural killer cells, B cells, and dendritic cells, which contrasted with very low levels of these cells in the prevaccination samples (figure 2A). As results for replicate biopsies for each condition clustered together, we pooled data for each condition for further analysis. In the tumor cell compartment, the fraction of proliferating tumor cells was reduced fivefold following vaccination (figure 2B). In the lung metastases, the postvaccination samples exhibited higher fractions of T cells, granzyme B+ cells, B cells, and dendritic cells (figure 2C), as well as a higher ratio of CD8+ T cells to regulatory T cells (figure 2D). In contrast, the prevaccination samples exhibited higher fractions of M2 macrophages and neutrophils (figure 2C). Further phenotypic analysis of T

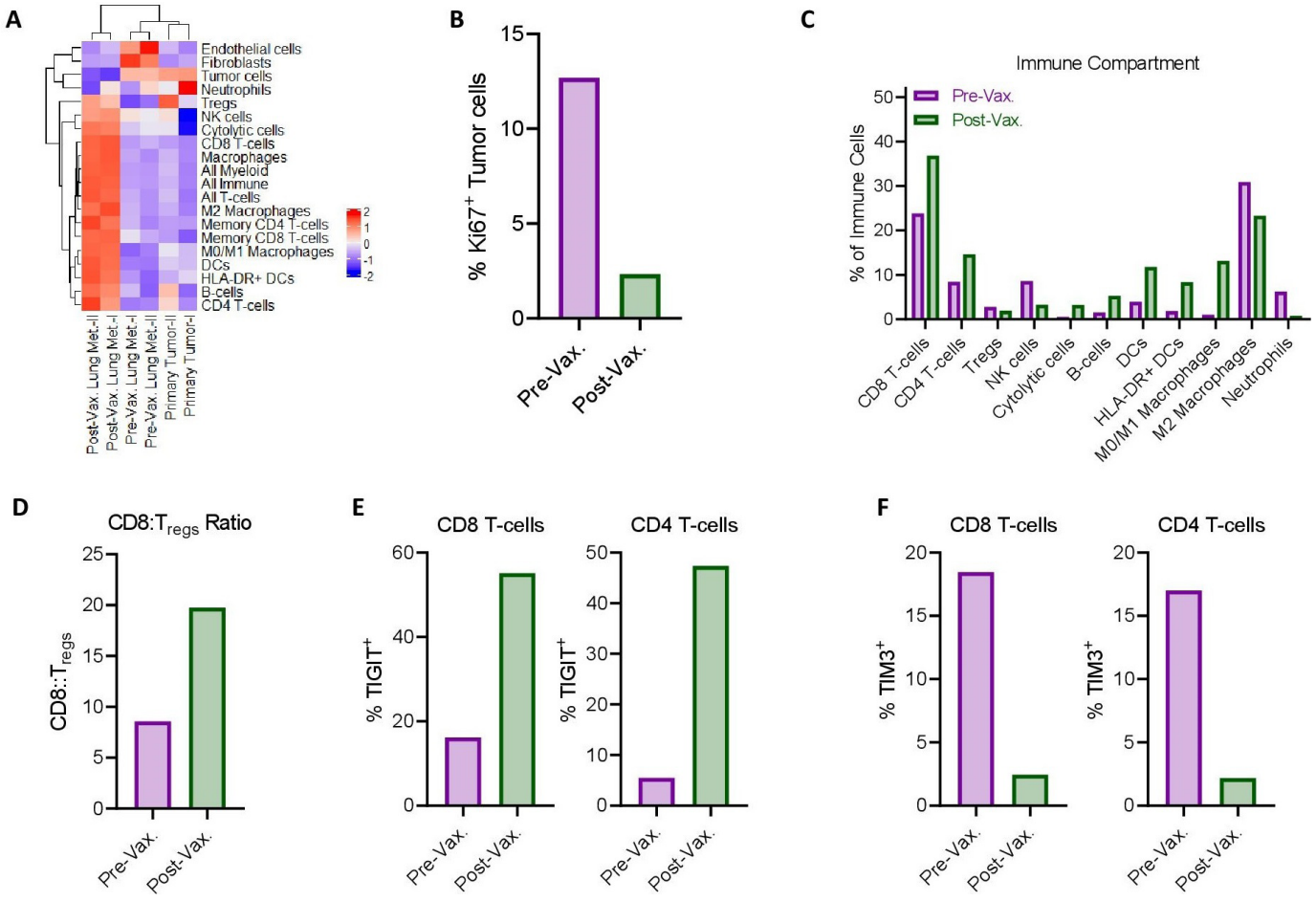

Figure 2 Imaging mass cytometry indicates robust anti-tumor immune response following COVID-19 vaccination. (A) Clustergram of imaging mass cytometry quantification in biopsy specimens from primary tumor and prevaccination (Pre-Vax.), and postvaccination (Post-Vax.) lung metastases (Lung Met.). I and II indicate specimens from different regions taken at the same time. Color axis represents each phenotype subpopulation frequency (z-normalized density [cells/mm^2] values), red for high frequency and blue for low frequency or absence (–2); (B) Percentage of proliferative (Ki67+) tumor cells (pan-CK+ and/or p63+) in Pre-Vax. and Post-Vax. lung metastasis specimens. (C) Percentage of indicated immune cell populations as percentage of total immune cells in Pre-Vax. and Post-Vax. lung metastasis specimens. (D–F) Comparison of Pre-Vax. and Post-Vax. lung metastasis specimens for (D) ratio of CD8+ T cells to regulatory T cells (Tregs), (E) percentages of CD8+ T cells and CD4+ T cells positive for TIGIT, and (F) percentages of CD8+ T cells and CD4+ T cells positive for TIM3. +, positive.

cells demonstrated that the percentage of cells expressing T-cell immunoglobulin and ITIM domain (TIGIT) was increased following vaccination (figure 2E), potentially indicative of antigen exposure.[5] Conversely, the percentage of T cells expressing the inhibitory receptor T-cell immunoglobulin and mucin domain-containing protein 3 (TIM3)[6] was decreased following vaccination (figure 2F). Taken together, these results suggest a robust anticancer immune response stimulated by COVID-19 vaccination with mRNA-1273.

DISCUSSION

Severe hyperinflammatory response occurs in a fraction of patients with COVID-19.[7] Similarly, COVID-19 vaccines have the potential to evoke intense immunologic responses.[8] Here, we describe a case of an anticancer response after COVID-19 vaccination. Histology analysis and tumor molecular profiling suggested that the primary tumor was poorly immunogenic, which is associated with poor responses to the most commonly used cancer immunotherapy. Notably, the patient reported grade 3 systemic adverse events after the second dose of the COVID-19 vaccine, which was preceded by spontaneous tumor regression, indicating that an intense inflammatory host response stimulated by the vaccine may have promoted an antitumor response.

The changes we observed in the TIME between the prevaccination and postvaccination tumor specimens, including increases in CD8+ and CD4+ T cell tumor infiltration and granzyme B+ cytolytic cells, are associated with immune cell activation. Moreover, we found notable reduction in the absolute number of tumor cells and the fraction of remaining cells actively proliferating, indicating an effective anti-cancer response, consistent with the patient's radiological findings.

CD8+ cytotoxic T cells have a pivotal role in the anti-cancer immune response; in fact, enhancing their activity is the main strategy of current successful cancer immunotherapies. Interestingly, although the efficacy of most vaccines is largely related to induction of antibody responses, T-cell-mediated immunity has emerged as an important mechanism of host defense against severe respiratory syndrome coronavirus-2[9]; COVID-19 vaccine has been shown to induce both virus-specific antibodies and T-cell responses,[9] which align with the TIME changes found in our analysis.

Dendritic cells, macrophages, and B cells are major populations of antigen-presenting cells critical for the initiation of adaptive immune response through T-cell activation, which is crucial for both vaccine-induced and anti-cancer immunity. Our finding of a substantial increase in antigen-presenting cell tumor infiltration in postvaccination samples is consistent with the robust innate and adaptative anticancer responses experienced by this patient.

Notably, we observed a shift in the TIME composition from myeloid predominant to lymphocytic predominant. Fractions of immune suppressive cells, represented by M2-macrophages, regulatory T cells, and cancer-associated fibroblasts, were higher in prevaccination samples than in postvaccination samples, which align with previous literature showing that immune suppressive cells are associated with immune evasion and worse prognosis in cancer.[10] Finally, dysfunctional and exhausted T cells, represented by expression for TIM3,[6] were also more prevalent in the pre-vaccination samples, whereas TIGIT expression in T cells was higher after vaccination and may be associated with T-cell activation.

In summary, this patient's clinical course and the analysis of prevaccination and postvaccination tumor samples support the hypothesis that stimulation of the innate immune system by the mRNA-1273 COVID-19 vaccine induced systemic immune activation and led to a robust and persistent anticancer response, represented by radiological tumor shrinkage and an 'anticancer' TIME composition. To our knowledge, this is the first reported case of COVID-19 vaccine-induced tumor regression and the first report of spontaneous tumor regression in a patient with salivary myoepithelial carcinoma. Host and tumor characteristics that led to this phenomenon remain unclear.

Author affiliations
[1]Thoracic and Head and Neck, The University of Texas MD Anderson Cancer Center, Houston, Texas, USA
[2]Systems Biology, The University of Texas MD Anderson Cancer Center, Houston, Texas, USA
[3]Translational Molecular Pathology, The University of Texas MD Anderson Cancer Center, Houston, Texas, USA
[4]Gynecologic Oncology and Reproductive Medicine, The University of Texas MD Anderson Cancer Center, Houston, Texas, USA
[5]Diagnostic Radiology, The University of Texas MD Anderson Cancer Center, Houston, Texas, USA
[6]Leukemia, The University of Texas MD Anderson Cancer Center, Houston, Texas, USA
[7]Pathology, City of Hope Comprehensive Cancer Center, Duarte, California, USA

Twitter Luana Guimaraes de Sousa @LGSousaMD

Acknowledgements We thank Stephanie Deming, scientific editor, Research Medical Library, for editing this article.

Contributors LGdS and DJM contibuted equally. All authors actively contributed to the manuscript development.

Funding DJM was supported by NCI grant K99CA240689. This work was supported by the National Institutes of Health/National Cancer Institute under award number P30CA016672, which supports the MD Anderson Cancer Center Imaging Core Facility and Research Histology Core Laboratory. JB is further supported by the NCI's Research Specialist 1 R50 CA243707-01A1. Bethyl Laboratories and Cell Signaling Technologies donated antibodies to the MD Anderson Flow Cytometry and Cellular Imaging Facility for use in IMC.

Competing interests RF: reports personal fees from Regeneron-Sanofi, Ayala Pharmaceuticals, Prelude Pharmaceuticals, Bicara Therapeutics, Klus Pharma, Medscape, Carevive, Merck, and Guidepoint Global and institutional fees from AstraZeneca, Merck, Genentech, Pfizer, EMD-Serono, Ayala Pharmaceuticals, Prelude Pharmaceuticals, and Rakuten Medical not related to the topic of the submitted work.

Patient consent for publication Consent obtained directly from patient(s).

Provenance and peer review Not commissioned; externally peer reviewed.

ORCID iDs
Luana Guimaraes de Sousa http://orcid.org/0000-0002-3516-7105
Jared Burks http://orcid.org/0000-0002-6173-9074

REFERENCES

1 Chapin-Bardales J, Gee J, Myers T. Reactogenicity following receipt of mRNA-based COVID-19 vaccines. *JAMA* 2021;325:2201–2.
2 Hervé C, Laupèze B, Del Giudice G, *et al*. The how's and what's of vaccine reactogenicity. *NPJ Vaccines* 2019;4:39.
3 Coley WB. The treatment of malignant tumors by repeated inoculations of erysipelas: with a report of ten original cases. *Am J Med Sci* 1893;105:487.
4 Guidance for industry: toxicity grading scale for healthy adult and adolescent volunteers enrolled in preventive vaccine clinical trials 2007.
5 Chauvin J-M, Zarour HM. TIGIT in cancer immunotherapy. *J Immunother Cancer* 2020;8:e000957.
6 Wolf Y, Anderson AC, Kuchroo VK. TIM3 comes of age as an inhibitory receptor. *Nat Rev Immunol* 2020;20:173–85.
7 Patel P, DeCuir J, Abrams J, *et al*. Clinical characteristics of multisystem inflammatory syndrome in adults: a systematic review. *JAMA Netw Open* 2021;4:e2126456.
8 Nune A, Iyengar KP, Goddard C, *et al*. Multisystem inflammatory syndrome in an adult following the SARS-CoV-2 vaccine (MIS-V). *BMJ Case Rep* 2021;14. doi:10.1136/bcr-2021-243888. [Epub ahead of print: 29 Jul 2021].
9 Zhuang Z, Lai X, Sun J. Mapping and role of T cell response in SARS-CoV-2-infected mice. *J Exp Med* 2021;218.
10 Whiteside TL. The tumor microenvironment and its role in promoting tumor growth. *Oncogene* 2008;27:5904–12.

THE UNIVERSITY OF TEXAS MD Anderson Cancer Center
Making Cancer History®

The University of Texas MD Anderson Cancer Center
1515 Holcombe Blvd., Houston, TX 77030

Print Date: 12/18/2020 15:30 CST
Location: MN Molecular Diag
Ordering: GONZALEZ PA,CIPRIANO C

Name: XXXXXX
MRN: XXXXXX
DOB/Age/Sex: X/XX/XXXX 60 years Female

Molecular Diagnostics

MD-20-124975

Solid Tumor Genomic Assay-DNA Report

Accession: MD-XX-XXXXX
Collection Date: 05/05/2020
Received In-lab Date: 11/25/2020 2:13 PM
Specimen Type: FFPE Slides
Pathology Accession for Source Material: XXX-XXXXXX 5 Outside Accession: XXX-XXXX
Histologic Diagnosis for Source Material (refer to source accession for details): Salivary carcinoma with myoepithelial differentiation
Control Source: PB

NAME XXXXX MRN XXXXXX MDL XXXXXXX

Solid Tumor Genomic Assay 2018 - DNA

Clinical test requisition for mutation studies on the following genes was received: *AKT1*, *BRAF*, *CDKN2A*

A next generation sequencing (NGS)-based analysis for the detection of somatic mutations in the coding sequence of 134 genes and selected copy number variations (amplifications) in 47 genes (overlap: 146 genes total) was performed on the DNA extracted from the sample in our CLIA-certified molecular diagnostics laboratory. Interpretative findings are reported in the gene summary table(s) below followed by specific details of detected sequence and/or copy number variants.

Interpretation Key:

Circled/Bold:	Mutation and/or amplification detected
Underlined:	Testing requested (ordered gene)
Asterisk:	Additional confirmation studies in progress

GENE SUMMARY:

THE UNIVERSITY OF TEXAS MD Anderson Cancer Center
Making Cancer History®

The University of Texas MD Anderson Cancer Center
1515 Holcombe Blvd., Houston, TX 77030

Print Date: 12/18/2020 15:30 CST
Location: MN Molecular Diag
Ordering: GONZALEZ PA,CIPRIANO C

Name: XXXXXX
MRN: XXXXXX
DOB/Age/Sex: X/XX/XXXX 60 years Female

Molecular Diagnostics

AKT1	*BTK*	*CREBBP*	*FGF19*	*HRAS*	*MAPK1*	*NBN*	*PIK3CB*	*RAF1*	*SPOP*
AKT2	*CBL*	*CSF1R*	*FGF3*	*IDH1*	*MAX*	*NF1*	*PIK3R1*	*RB1*	*SRC*
AKT3	*CCND1*	*CTNNB1*	*FGFR1*	*IDH2*	*MDM2*	*NF2*	*PMS2*	*RET*	*STAT3*
ALK	*CCND2*	*DDR2*	*FGFR2*	*IGF1R*	*MDM4*	*NFE2L2*	*POLE*	*RHEB*	*STK11*
AR	*CCND3*	*EGFR*	*FGFR3*	*JAK1*	*MED12*	*NOTCH1*	*PPARG*	*RHOA*	*TERT*
ARAF	*CCNE1*	*ERBB2*	*FGFR4*	*JAK2*	*MET*	*NOTCH2*	*PPP2R1A*	*RICTOR*	*TOP1*
ARID1A	*CDK12*	*ERBB3*	*FLT3*	*JAK3*	*MLH1*	***NOTCH3***	*PTCH1*	*RNF43*	***TP53***
ATM	*CDK2*	*ERBB4*	*FOXL2*	*KDR*	*MRE11A*	*NRAS*	*PTEN*	*ROS1*	*TSC1*
ATR	*CDK4*	*ERCC2*	*GATA2*	*KIT*	*MSH2*	*NTRK1*	*PTPN11*	*SETD2*	*TSC2*
ATRX	*CDK6*	*ESR1*	*GNA11*	*KNSTRN*	*MSH6*	*NTRK2*	*RAC1*	*SF3B1*	*U2AF1*
AXL	*CDKN1B*	*EZH2*	*GNAQ*	*KRAS*	*MTOR*	*NTRK3*	*RAD50*	*SLX4*	*XPO1*
BAP1	*CDKN2A*	*FANCA*	*GNAS*	*MAGOH*	*MYC*	*PALB2*	*RAD51*	*SMAD4*	
BRAF	*CDKN2B*	*FANCD2*	*H3F3A*	*MAP2K1*	*MYCL*	*PDGFRA*	*RAD51B*	*SMARCA4*	
BRCA1	*CHEK1*	*FANCI*	*HIST1H3B*	*MAP2K2*	*MYCN*	*PDGFRB*	*RAD51C*	*SMARCB1*	
BRCA2	*CHEK2*	*FBXW7*	*HNF1A*	*MAP2K4*	*MYD88*	*PIK3CA*	*RAD51D*	*SMO*	

FINDINGS:

Copy Number Variations
None identified

Somatic Mutations***

Gene	Standardized Nomenclature (HGVS)	Location	DNA change	Protein change	COSMIC ID	VAF*
NOTCH3	NM_000435.2(NOTCH3):c.5086C>T p.P1696S	Exon 27	SNV	Missense		4.3%
TP53	NM_000546.5(TP53):c.702C>G p.Y234*	Exon 7	SNV	Nonsense	COSM44785	6%

*** These mutations are present at low allelic frequencies compared to estimated tumor cellularity. The assay was repeated twice.* VAF, variant allele frequency

THE UNIVERSITY OF TEXAS MD Anderson Cancer Center
Making Cancer History®

The University of Texas MD Anderson Cancer Center
1515 Holcombe Blvd., Houston, TX 77030

Print Date: 12/18/2020 15:30 CST
Location: MN Molecular Diag
Ordering: GONZALEZ PA,CIPRIANO C

Name: XXXXXX
MRN: XXXXXX
DOB/Age/Sex: X/XX/XXXX 60 years Female

Molecular Diagnostics

GUIDE TO STANDARDIZED NOMENCLATURE AND EXPLANATION OF CHANGES:

Mutations identified are described using an implementation of a standardized nomenclature developed by the Human Genome Variation Society (HGVS, <http://www.hgvs.org/mutnomen/>).

The normative Genbank gene reference sequence identifier and gene symbol in parentheses are provided, followed by the coding DNA sequence change (e.g., "c. 200A>G", which would mean that the position 200 adenine is changed to guanine), and then the inferred protein change (e.g., "p. V35C", which would mean that the amino acid at codon 35 is changed from valine to cysteine).

Additional explanations for the DNA and protein changes seen in the current specimen are shown in the following tables:

Explanation of DNA variant/mutation types seen in this specimen

DNA Change	
SNV	A single nucleotide difference (point mutation) has been identified in the patient sample relative to the reference wild-type gene sequence

Explanation of protein variant/mutation types seen in this specimen

Protein Change	
Missense	A single amino acid residue change in the patient sample relative to the reference wild-type protein sequence
Nonsense	A single nucleotide change resulting in a premature stop codon leading to a truncated protein product in the patient sample relative to the reference wild-type protein sequence

ADDITIONAL INFORMATION ON GENES WITH FINDINGS IDENTIFIED ON THIS ASSAY

NOTCH3	http://www.genenames.org/data/hgnc_data.php?hgnc_id=7883
TP53	http://www.genenames.org/data/hgnc_data.php?hgnc_id=11998

METHODOLOGY:

Test Platform: PCR-based sequencing is performed using a next generation sequencing (NGS) platform on genomic DNA to screen for mutations and copy number amplifications in the coding sequences of genes listed below. NGS sequencing analysis of these genes was further confirmed by other platforms during validation in our CLIA-certified molecular diagnostics laboratory. The genomic reference sequence used is GRCh37/hg19. Detailed information about

THE UNIVERSITY OF TEXAS MD Anderson Cancer Center
Making Cancer History®

The University of Texas MD Anderson Cancer Center
1515 Holcombe Blvd., Houston, TX 77030

Print Date: 12/18/2020 15:30 CST
Location: MN Molecular Diag
Ordering: GONZALEZ PA,CIPRIANO C

Name: XXXXXX
MRN: XXXXXX
DOB/Age/Sex: X/XX/XXXX 60 years Female

Molecular Diagnostics

the signal-processing, base calling, alignment, variant calling, and copy number calling algorithms are available upon request.

Analytical sensitivity and additional details: For this assay, sensitivity of detection is related in part to depth of coverage, tumor percentage, and allelic frequency for the mutation. Although the NGS platform is capable of achieving a much higher analytical sensitivity; for clinical purposes, we determined the effective lower limit of detection of this assay (analytical sensitivity) for single nucleotide variations to be in the range of 5% (one mutant allele in the background of nineteen wild type alleles) to 10% (one mutant allele in the background of nine wild type alleles) by taking into consideration the depth of coverage at a given base and the ability to confirm low level mutations using independent conventional platforms. Sensitivity for amplifications depends on both input tumor percentage and the amplitude of the gene amplification. We require a minimum of 20% tumor nuclei in the sample to reduce the potential for false-negative results. The analytic pipeline in this assay attempts to normalize for inter-amplicon performance differences and total sample loading, but does not attempt to correct for tumor percentage. A nominal threshold of 7 for the estimated copy number is used to restrict reporting to high-confidence amplification calls.

Details and limitations of the test:

- Matched non-tumor tissue from this patient has been tested and germline variants have been excluded.
- The primary purpose of this panel is to detect somatic mutations in genes involved in oncogenesis of this patient's tumor. This panel is not designed to detect germline variants for familial tumors, and the test or results thereof should not be used to detect germline variants for hereditary cancer syndromes.
- The assay is designed to detect point mutations, small insertion/deletions, and copy number gains (amplifications).
- Variants detected at very low allelic frequencies not deemed to be confirmable by independent, orthogonal methods and/or in significant discordance with the percentage of tumor in the tested sample may be excluded as the clinical significance and reliability of such low level variant calls is not clear.
- Copy number assessment by next generation sequencing can be affected by tumor percentage, amplitude of gene amplification, enrichment of tumor during pre-analytical phase, library preparation methods and analysis algorithms. False negative results can be obtained in cases with low tumor percentage, low amplicon coverage and/or borderline copy number gains. Correlation with traditional methods of copy number assessment such as fluorescent in situ hybridization (FISH) is recommended as applicable

Report annotation and generation software: A post-variant calling analysis and annotation tool, OncoSeek version 1.8.1.490, was used in the construction of this report.

THE UNIVERSITY OF TEXAS MD Anderson Cancer Center
Making Cancer History®

The University of Texas MD Anderson Cancer Center
1515 Holcombe Blvd., Houston, TX 77030

Print Date: 12/18/2020 15:30 CST
Location: MN Molecular Diag
Ordering: GONZALEZ PA,CIPRIANO C

Name: XXXXXX
MRN: XXXXXX
DOB/Age/Sex: X/XX/XXXX 60 years Female

Molecular Diagnostics

Sequencing coverage of the genes: The following table describes adequacy of coverage in this assay across the full set of covered genes, exons, and codons, for genes with exon-level sequencing on this assay. Adequately covered amplicons are defined as those having total coverage depth of greater than or equal to 250 reads, or for which an orthogonal mutation analysis testing has been performed. Presence of mutations outside the tested regions listed below cannot be ruled out.

Coverage by gene and codon(s) tested for adequate amplicons

Gene	Exons (codons) tested
AKT1 (NM_005163)	3 (16-56), 4 (59-96), 6 (146-149), 6-7 (177-195), 9 (235-274), 11 (320-380), 12 (391-411), 13 (450-455), 14 (459-481)
AKT2 (NM_001626)	3 (16-55), 4 (76-96), 6 (148-153), 7 (192-210), 8 (221-236), 10 (278-279), 11 (322-381), 12 (395-421), 14 (456-482)
AKT3 (NM_005465)	2 (16-28), 2 (48-58), 3 (66-95), 4 (123-143), 6 (188-209), 8 (233-267), 10 (317-367), 11 (388-399)
ALK (NM_004304)	20-28 (1096-1388)
AR (NM_000044)	1 (1-45), 1 (135-178), 1 (245-285), 1 (342-388), 3 (615-629), 4 (707-725), 6-7 (797-831), 8 (870-910)
ARAF (NM_001654)	7 (186-216)
ARID1A (NM_006015)	1 (28-73), 1 (106-151), 1-8 (161-838), 8-20 (861-2062), 20 (2081-2286)
ATM (NM_000051)	2-17 (1-865), 18-19 (880-974), 20-25 (1001-1249), 26 (1258-1283), 26-44 (1292-2136), 44-46 (2146-2262), 47-49 (2270-2389), 49-51 (2414-2542), 52-54 (2544-2667), 55 (2671-2711), 56-57 (2718-2806), 58-63 (2823-3028), 63 (3041-3057)
ATR (NM_001184)	1-5 (1-450), 6-8 (458-582), 8 (584-629), 9-13 (636-882), 13-15 (896-1052), 16-19 (1058-1237), 20 (1242-1262), 21-27 (1274-1618), 28-29 (1628-1692), 29-34 (1705-1965), 35-38 (1967-2184), 39-40 (2187-2296), 41-47 (2300-2645)
ATRX (NM_000489)	1-8 (1-221), 9-11 (257-1301), 12-16 (1315-1562), 17-18 (1567-1644), 19-21 (1653-1766), 21-28 (1785-2108), 29-35 (2117-2493)
AXL (NM_001699)	1 (1-29), 3 (103-137), 6 (223-261), 7 (288-332), 8 (351-378), 9 (386-429), 11 (473-497), 12 (516-536), 15 (593-633), 17 (670-686), 19 (769-782)
BAP1 (NM_004656)	1-17 (6-730)
BRAF (NM_004333)	11-18 (439-722)
BRCA1 (NM_007294)	2-7 (1-183), 8-23 (191-1864)
BRCA2 (NM_000059)	2-10 (1-280), 10-27 (294-3419)
BTK (NM_000061)	7 (174-196), 15 (457-498)
CBL (NM_005188)	8-9 (366-435), 9 (446-477)
CCND1 (NM_053056)	1 (1-10), 1-2 (14-81), 2 (91-138), 3 (142-192), 4-5 (199-291)
CCND2 (NM_001759)	1-2 (1-80), 2-3 (116-191), 4-5 (195-282)
CCND3 (NM_001760)	1-2 (53-122), 3 (139-180), 4 (192-237), 5 (250-293)
CCNE1 (NM_001238)	4-5 (39-92), 6-9 (127-258), 11-12 (348-411)
CDK12 (NM_016507)	1 (1-42), 1-14 (71-1491)

THE UNIVERSITY OF TEXAS MD Anderson Cancer Center
Making Cancer History®

The University of Texas MD Anderson Cancer Center
1515 Holcombe Blvd., Houston, TX 77030

Print Date: 12/18/2020 15:30 CST
Location: MN Molecular Diag
Ordering: GONZALEZ PA,CIPRIANO C

Name: XXXXXX
MRN: XXXXXX
DOB/Age/Sex: X/XX/XXXX 60 years Female

Molecular Diagnostics

CDK2 (NM_001798)	1-2 (1-45), 4 (106-153), 5-6 (163-228), 6-7 (252-297)
CDK4 (NM_000075)	2-3 (17-116), 4 (119-163), 5-6 (175-228), 7-8 (268-304)
CDK6 (NM_001259)	2 (7-75), 3 (78-86), 3 (104-123), 4 (136-179), 5 (183-216), 6 (221-233), 7-8 (236-287), 8 (315-327)
CDKN1B (NM_004064)	1-2 (1-199)
CDKN2A (NM_000077)	1-2 (1-90), 2 (98-140), 2-3 (143-157)
CDKN2B (NM_004936)	1-2 (1-139)
CHEK1 (NM_001274)	2-10 (1-334), 10-13 (363-477)
CHEK2 (NM_007194)	11 (366-420), 15 (515-544)
CREBBP (NM_004380)	1-3 (1-325), 4-5 (356-444), 6-31 (476-1933), 31 (1961-2443)
CSF1R (NM_005211)	7 (297-319), 11 (517-542), 22 (963-973)
CTNNB1 (NM_001904)	3 (5-67), 7 (327-361)
DDR2 (NM_006182)	5 (97-139), 8 (228-279), 13-18 (540-856)
EGFR (NM_005228)	3 (84-125), 7 (281-297), 12 (452-494), 15 (582-625), 18-20 (688-801), 20-24 (807-977)
ERBB2 (NM_004448)	8 (301-327), 17 (649-680), 18-24 (696-990)
ERBB3 (NM_001982)	2-3 (48-118), 6 (207-243), 7-8 (270-326), 9 (330-350), 23 (898-934)
ERBB4 (NM_005235)	12 (437-478), 17 (649-671), 18 (694-726), 20 (781-823), 28 (1194-1236)
ERCC2 (NM_000400)	3 (36-47), 5 (84-114), 8 (223-240), 15 (460-492), 21 (658-682)
ESR1 (NM_000125)	1 (1-42), 1 (53-99), 2 (184-215), 3 (232-254), 4 (268-340), 5 (367-412), 7 (457-518), 8 (532-574)
EZH2 (NM_004456)	16 (639-649), 18 (677-704)
FANCA (NM_000135)	1-43 (1-1456)
FANCD2 (NM_033084)	2-15 (1-409), 15-19 (423-589), 21-28 (610-904), 29 (906-927), 29-43 (948-1472)
FANCI (NM_018193)	2-37 (1-1269)
FBXW7 (NM_033632)	2-4 (1-242), 5-9 (255-473), 10 (478-509), 10-12 (522-708)
FGF19 (NM_005117)	1 (1-33), 2-3 (78-217)
FGF3 (NM_005247)	1-3 (1-217), 3 (229-240)
FGFR1 (NM_015850)	4 (120-148), 6 (217-247), 8 (311-355), 9 (408-426), 12 (516-553), 14 (642-657), 16 (709-727), 18 (786-821)
FGFR2 (NM_000141)	6 (209-235), 7 (250-273), 7-8 (277-350), 9 (362-399), 10 (453-480), 12 (521-558), 13 (589-621), 14-15 (631-686), 16 (699-730), 18 (768-804)
FGFR3 (NM_000142)	2 (1-37), 4 (127-133), 8 (329-359), 9 (368-412), 10 (423-439), 14 (633-653), 15-16 (659-719)
FGFR4 (NM_022963)	1 (1-31), 2 (72-116), 4 (163-199), 6 (243-283), 8 (359-392), 10-11 (467-535), 13 (609-632), 15 (683-713)
FLT3 (NM_004119)	3 (93-123), 6 (205-213), 8 (302-346), 10 (402-435), 12 (502-533), 15 (613-648), 18 (742-764), 20-21 (808-885), 24 (957-994)
FOXL2 (NM_023067)	1 (94-137)
GATA2 (NM_032638)	4 (291-330), 5 (341-379), 6 (452-481)
GNA11 (NM_002067)	4 (165-196), 5 (205-240)
GNAQ (NM_002072)	2 (60-100), 4-5 (163-224)

THE UNIVERSITY OF TEXAS MD Anderson Cancer Center
Making Cancer History®

The University of Texas MD Anderson Cancer Center
1515 Holcombe Blvd., Houston, TX 77030

Print Date: 12/18/2020 15:30 CST
Location: MN Molecular Diag
Ordering: GONZALEZ PA,CIPRIANO C

Name: XXXXXX
MRN: XXXXXX
DOB/Age/Sex: X/XX/XXXX 60 years Female

Molecular Diagnostics

GNAS (NM_000516)	8 (196-218), 9 (220-240)
H3F3A (NM_002107)	2 (1-36)
HIST1H3B (NM_003537)	1 (6-37), 1 (61-102)
HNF1A (NM_000545)	2 (109-116), 3 (196-238)
HRAS (NM_005343)	2 (6-34), 3 (44-87), 4 (97-150)
IDH1 (NM_005896)	4 (100-138)
IDH2 (NM_002168)	4 (125-155), 4 (162-178)
IGF1R (NM_000875)	1 (1-32), 2 (138-176), 4 (318-328), 6 (416-457), 8 (572-608), 10 (674-711), 12 (829-865), 14 (928-946), 17 (1063-1099), 20 (1196-1220)
JAK1 (NM_002227)	14 (634-663), 15-16 (668-743)
JAK2 (NM_004972)	14 (600-622)
JAK3 (NM_000215)	11-12 (502-563), 15 (639-683)
KDR (NM_002253)	11 (482-512), 16 (766-791), 23 (1026-1064), 24 (1082-1102)
KIT (NM_000222)	8 (411-445), 9 (487-514), 10-20 (516-934)
KNSTRN (NM_033286)	1 (1-28)
KRAS (NM_004985)	2-3 (1-93), 4-5 (97-189)
MAGOH (NM_002370)	5 (114-147)
MAP2K1 (NM_002755)	2 (27-96), 3 (98-135), 6 (190-227), 11 (357-394)
MAP2K2 (NM_030662)	3 (102-123)
MAP2K4 (NM_003010)	4 (132-154), 5 (178-208)
MAPK1 (NM_002745)	7 (300-322)
MAX (NM_002382)	3 (22-56), 4 (58-83)
MDM2 (NM_002392)	2 (22-33), 3 (51-58), 4 (79-103), 7 (160-175), 8 (198-228), 9 (236-267), 10 (289-306), 11 (340-373), 11 (406-439)
MDM4 (NM_002393)	2 (1-17), 3 (27-50), 5-6 (96-137), 7 (158-171), 8 (212-224), 9 (229-269), 11 (302-334), 11 (348-386), 11 (428-459)
MED12 (NM_005120)	2 (34-59), 26 (1199-1227)
MET (NM_001127500)	2 (151-192), 2 (217-257), 2 (287-331), 2 (344-384), 14 (981-989), 14-21 (1003-1367)
MLH1 (NM_000249)	1-19 (1-757)
MRE11A (NM_005590)	2 (1-7), 3-19 (20-681)
MSH2 (NM_000251)	1-4 (1-259), 5 (265-307), 6-10 (315-521), 11-15 (554-852), 16 (879-935)
MSH6 (NM_000179)	1-10 (1-1361)
MTOR (NM_004958)	29 (1418-1443), 30 (1452-1490), 31 (1509-1524), 39 (1789-1803), 40 (1876-1905), 43 (1971-1994), 43-44 (1999-2035), 47-48 (2187-2251), 53 (2394-2434), 56-57 (2483-2520)
MYC (NM_002467)	1-2 (1-87), 2 (98-131), 2 (140-185), 2 (196-226), 3 (268-278), 3 (297-340), 3 (352-395), 3 (413-453)
MYCL (NM_005376)	2 (60-96), 2 (163-237)
MYCN (NM_005378)	2 (1-125), 2-3 (229-349), 3 (371-450)
MYD88 (NM_002468)	3 (181-221), 5 (259-269)

THE UNIVERSITY OF TEXAS MD Anderson Cancer Center
Making Cancer History®

The University of Texas MD Anderson Cancer Center
1515 Holcombe Blvd., Houston, TX 77030

Print Date: 12/18/2020 15:30 CST
Location: MN Molecular Diag
Ordering: GONZALEZ PA,CIPRIANO C

Name: XXXXXX
MRN: XXXXXX
DOB/Age/Sex: X/XX/XXXX 60 years Female

Molecular Diagnostics

NBN (NM_002485)	1-5 (1-166), 6-16 (200-755)
NF1 (NM_001042492)	1-16 (1-596), 17-23 (616-1038), 25-58 (1071-2840)
NF2 (NM_000268)	1-10 (1-332), 11-16 (334-596)
NFE2L2 (NM_006164)	2 (23-59), 2 (74-104)
NOTCH1 (NM_017617)	2-27 (21-1680), 27 (1686-1723), 28-34 (1736-2116), 34 (2145-2556)
NOTCH2 (NM_024408)	1 (1-25), 3 (68-131), 4 (139-191), 4-34 (193-2472)
NOTCH3 (NM_000435)	1-2 (16-48), 3-18 (66-959), 18-24 (969-1292), 24 (1414-1449), 25-26 (1468-1631), 27-33 (1659-2153), 33 (2163-2322)
NRAS (NM_002524)	2 (1-22), 3 (49-89), 4 (110-150)
NTRK1 (NM_002529)	2 (71-92), 3 (106-120), 6 (192-227), 8 (321-393), 11 (418-446), 14 (553-599), 15 (658-682), 17 (747-790)
NTRK2 (NM_006180)	4 (1-43), 6 (96-120), 9 (197-239), 11 (294-366), 14 (433-466), 16 (490-531), 17 (580-588), 18 (601-641), 19 (674-723), 20 (725-756)
NTRK3 (NM_002530)	7 (155-161), 10 (303-318), 10 (377-402), 13 (432-456), 14 (472-518), 16 (576-630), 17 (662-711), 19 (808-826)
PALB2 (NM_024675)	1-3 (1-71), 4-6 (79-862), 7-13 (888-1187)
PDGFRA (NM_006206)	12-15 (552-719), 17-21 (775-960)
PDGFRB (NM_002609)	2 (1-14), 3 (99-122), 5 (211-235), 7 (333-370), 9 (450-456), 11 (527-545), 12-13 (587-638), 16 (753-782), 19 (881-900), 22 (969-1009), 23 (1093-1107)
PIK3CA (NM_006218)	2 (1-5), 2-3 (77-138), 5 (311-351), 8 (418-457), 10-11 (532-582), 14 (693-729), 21 (1015-1057)
PIK3CB (NM_006219)	1 (31-57), 3 (138-174), 5 (268-294), 7 (400-434), 10 (518-527), 11 (545-586), 14 (679-683), 16 (784-809), 20 (933-954), 22 (1026-1071)
PIK3R1 (NM_181523)	2-11 (1-437), 11-16 (440-725)
PMS2 (NM_000535)	1-2 (1-30), 2-5 (35-165), 6-11 (180-657), 12 (669-680), 12-13 (716-726), 15 (855-863)
POLE (NM_006231)	1-36 (1-1531), 36-46 (1540-2177), 47-49 (2217-2287)
PPARG (NM_015869)	1 (1-28), 2 (53-78), 3 (104-134), 3 (152-160), 4 (169-200), 5 (207-228), 5 (257-273), 6 (282-321), 6 (350-390), 7 (424-461)
PPP2R1A (NM_014225)	5 (172-199), 6 (220-263)
PTCH1 (NM_000264)	1-23 (6-1344), 23 (1374-1448)
PTEN (NM_000314)	1-9 (1-382)
PTPN11 (NM_002834)	3 (52-91), 13 (485-527)
RAC1 (NM_006908)	2 (18-36)
RAD50 (NM_005732)	1-5 (1-244), 6-9 (253-478), 10 (485-545), 11-12 (553-657), 13-16 (681-902), 17-19 (907-980), 19-23 (987-1206), 24-25 (1212-1313)
RAD51 (NM_002875)	2-4 (1-115), 5-10 (121-340)
RAD51B (NM_133509)	2-5 (1-113), 5-7 (142-245), 8-11 (253-374)
RAD51C (NM_002876)	1-2 (1-136)
RAD51D (NM_133629)	1-7 (1-217)
RAF1 (NM_002880)	7 (235-276), 12 (407-442)
RB1 (NM_000321)	1-2 (1-85), 3-4 (89-159), 5-6 (167-194), 6-15 (196-464), 16-18 (480-582), 18-21 (587-736), 22-27 (743-929)

THE UNIVERSITY OF TEXAS MD Anderson Cancer Center
Making Cancer History®

The University of Texas MD Anderson Cancer Center
1515 Holcombe Blvd., Houston, TX 77030

Print Date: 12/18/2020 15:30 CST
Location: MN Molecular Diag
Ordering: GONZALEZ PA,CIPRIANO C

Name: XXXXXX
MRN: XXXXXX
DOB/Age/Sex: X/XX/XXXX 60 years Female

Molecular Diagnostics

RET (NM_020975)	10-11 (609-654), 12-14 (713-869), 15-18 (875-1013)
RHEB (NM_005614)	2 (18-42)
RHOA (NM_001664)	2 (2-44)
RICTOR (NM_152756)	7 (153-175), 10 (291-297), 16 (462-467), 21 (658-684), 26 (834-863), 30 (981-1019), 31 (1210-1246), 32 (1382-1416), 35 (1588-1597), 38 (1690-1709)
RNF43 (NM_017763)	2-9 (1-442), 9-10 (455-784)
ROS1 (NM_002944)	36-38 (1926-2045), 39-40 (2050-2092), 40-42 (2106-2245)
SETD2 (NM_014159)	1-11 (1-1799), 12-21 (1809-2565)
SF3B1 (NM_012433)	14 (603-640), 14 (655-679), 15 (693-716), 15-16 (738-747)
SLX4 (NM_032444)	2-12 (1-1477), 12-15 (1493-1835)
SMAD4 (NM_005359)	9 (335-375), 10 (380-401), 12 (519-553)
SMARCA4 (NM_003072)	2-12 (1-644), 13-15 (648-756), 16-19 (759-936), 20-25 (954-1162), 26-35 (1183-1648)
SMARCB1 (NM_003073)	1-2 (1-72), 3-5 (78-206), 6-9 (210-386)
SMO (NM_005631)	3 (186-228), 4-5 (263-354), 6 (397-422), 9 (511-551), 11 (608-646)
SPOP (NM_003563)	5 (88-118), 6 (125-160)
SRC (NM_005417)	12 (374-418)
STAT3 (NM_139276)	13 (398-411), 20 (583-620), 21 (630-667)
STK11 (NM_000455)	1-8 (1-361), 9 (370-434)
TERT (NM_198253)	1 (1-18), 2 (267-310), 2 (394-425), 3 (553-585), 4 (626-650), 6 (718-762), 9 (823-852), 11 (920-948), 14 (1011-1043), 16 (1099-1133)
TOP1 (NM_003286)	20 (682-722)
TP53 (NM_000546)	2-11 (1-394)
TSC1 (NM_000368)	3-23 (1-1165)
TSC2 (NM_000548)	2-35 (1-1523), 37-39 (1555-1690), 40-42 (1706-1808)
U2AF1 (NM_006758)	2 (15-41), 6 (137-161)
XPO1 (NM_003400)	15 (563-575)

DISCLAIMER:

This test was developed and its performance characteristics determined by the Molecular Diagnostic Laboratory (MDL) at the M.D. Anderson Cancer Center. It has not been cleared by the U.S. Food and Drug Administration. However, such approval is not required for clinical implementation, and the test results on the ordered genes have been shown to be clinically useful. This laboratory is CAP accredited and CLIA certified to perform high complexity molecular testing for clinical purposes.

THE UNIVERSITY OF TEXAS MD Anderson Cancer Center
Making Cancer History®

The University of Texas MD Anderson Cancer Center
1515 Holcombe Blvd., Houston, TX 77030

Print Date: 12/18/2020 15:30 CST
Location: MN Molecular Diag
Ordering: GONZALEZ PA,CIPRIANO C

Name: XXXXXX
MRN: XXXXXX
DOB/Age/Sex: X/XX/XXXX 60 years Female

Molecular Diagnostics

Electronically Signed By: ASIF RASHID, MD - 10160 and reported on 12/18/20 15:30 PM

Test performed by:
The University of Texas MD Anderson Cancer Center Molecular Diagnostic Lab
6565 MD Anderson Blvd
Houston, TX 77030

THE UNIVERSITY OF TEXAS
MD Anderson Cancer Center

Department of Pathology
1515 Holcombe Boulevard, Unit 0085
Houston, Texas 77030-4095
Tel: 713-792-3205 Fax: 713-794-4630

Pathology Report
X20-019508

XXXXXXXX
XXXXXXXX
DOB: X/XX/XXXX
Sex: Female

Collected: 5/5/2020
Received: 8/28/2020 11:54 AM

Case Type: Outside

Submitting Provider:
Stephanie Anne Rosen, MD

Addended Report: OUTSIDE

Materials Received

Accession#, Stained, Block, Unstained	Collected	Received
A. XXX-XXXX, 0 SS, 1 BLOCK, 0 USS	5/5/2020	8/28/2020

Addendum 1

Addendum to report additional testing performed and interpreted at MDACC at request of treating physician:

PD-L1 (clone 22C3) by immunohistochemistry NOT EXPRESSED/NEGATIVE. The Combined Positive Score (CPS) is less than 1.

Addendum electronically signed by Adel K. El-Naggar, MD on 3/2/2021 at 10:51 AM

Diagnosis

One outside paraffin block (XXXXX):

Parotid gland, left, parotidectomy (representative #5):

HIGH-GRADE CARCINOMA WITH MYOEPITHELIAL DIFFERENTIATION, See comment.
Size:at least 3 cm by report
Lymphovascular invasion, present, multifocal
Perineural invasion: not evaluable
Margins: EXTENDING TO INKED RESECTION MARGIN.

Electronically signed by Michelle Williams, MD on 9/7/2020 at 1:23 AM

Comment

The tumor is high-grade thought fairly monomorphic with areas of necrosis. Immunohistochemical stains performed at MD Anderson Cancer Center show that the neoplastic cells are strongly immunoreactive to CK7, p40, Bcl-2 and SMA, while showing no expression for DOG-1. Per outside report (slides not received/reviewed), the neoplastic cells were negative for HER2, AR, SOX10, S100, mammoglobin, c-kit and GFAP. Ki-67 stain showed proliferation in 20% of neoplastic cells.

The features are compatible with a salivary primary. No definitive precursor lesion seen on representative sections though this could have arising as a carcinoma -ex pleomorphic adenoma or high-grade transformation from a pre-existing process. Clinical correlation is advised.

Disclaimer

"Some tests reported here may have been developed and performance characteristics determined by UT MD Anderson Pathology and Laboratory Medicine. These tests have not been specifically cleared or approved by the U.S. Food and Drug Administration. If applicable, controls were reviewed and showed appropriate reactivity."

THE UNIVERSITY OF TEXAS
MD Anderson Cancer Center

Department of Pathology
1515 Holcombe Boulevard, Unit 0085
Houston, Texas 77030-4095
Tel: 713-792-3205 Fax: 713-794-4630

Pathology Report
X20-019508

XXXXXXXX
XXXXXXXX
DOB: X/XX/XXXX
Sex: Female

Collected: 5/5/2020
Received: 8/28/2020 11:54 AM

Case Type: Outside

Submitting Provider:
Stephanie Anne Rosen, MD

THE UNIVERSITY OF TEXAS
MD Anderson Cancer Center
Making Cancer History®

The University of Texas MD Anderson Cancer Center
1515 Holcombe Blvd., Houston, TX 77030

Print Date: 12/8/2020 10:25 CST
Location: MN Molecular Diag
Ordering: GONZALEZ PA,CIPRIANO C

NAME: XXXXX
MRN: XXXXX
DOB/Age/Sex: X/XX/XXXX 60 years Female

Molecular Diagnostics

MD- XXXXXX

Solid Tumor Genomic Assay-Fusions Report

Accession: MD-20-XXXXX
Collection Date: 05/05/2020
Received In-lab Date: 11/25/2020 2:13 PM
Specimen Type: FFPE Slides
Pathology Accession for Source Material: XX-XXXX 5 Outside Accession: XXX-XXXX
Histologic Diagnosis for Source Material (refer to source accession for details): Salivary carcinoma with myoepithelial differentiation

NAME XXXXX MRN XXXXX MDL XXXXX

Solid Tumor Genomic Assay 2018 - RNA (Fusions)

Clinical test requisition for fusion studies on the following genes was received: *NTRK1*, *NTRK2*, *NTRK3*

A next generation sequencing (NGS)-based analysis for the detection of targeted inter- and intragenic fusions involving 51 genes was performed.

FINDINGS:

Gene Fusions
None identified

Unless otherwise noted, all labs were performed at MD Anderson

THE UNIVERSITY OF TEXAS
MD Anderson Cancer Center
Making Cancer History®

The University of Texas MD Anderson Cancer Center
1515 Holcombe Blvd., Houston, TX 77030

Print Date: 12/8/2020 10:25 CST
Location: MN Molecular Diag
Ordering: GONZALEZ PA,CIPRIANO C

NAME: XXXXX
MRN: XXXXX
DOB/Age/Sex: X/XX/XXXX 60 years Female

Molecular Diagnostics

METHODOLOGY:

Test platform: cDNA prepared from extracted RNA is combined with targeted amplicon based next generation sequencing (NGS) to amplify both a set of expected control RNA sequences and a set of targeted fusion sequences corresponding to clinically relevant known inter- and intragenic fusions in 51 genes (*AKT2, ALK, AR, AXL, BRAF, BRCA1, BRCA2, CDKN2A, EGFR, ERB84, ERBB2, ERG, ESR1, ETV1, ETV4, ETV5, FGFR1, FGFR2, FGFR3, FGR, FLT3, JAK2, KRAS, MDM4, MET, MYB, MYBL1, NF1, NOTCH1, NOTCH4, NRG1, NTRK1, NTRK2, NTRK3, NUTM1, PDGFRA, PDGFRB, PIK3CA, PPARG, PRKACA, PRKACB, PTEN, RAD51B, RAF1, RB1, RELA, RET, ROS1, RSPO2, RSPO3,* and *TERT*). Sequences are aligned against a synthetic fusion genome and fusions are identified by coverage analysis. Detailed information about the signal-processing, base calling, alignment, and fusion calling including specific fusion partners and break-points, are available upon request.

Analytical sensitivity and additional details: Assessing sensitivity/limit of detection for a non-cellular fusion assay is challenging because fusion messenger RNA is likely to be expressed idiosyncratically and non-uniformly with respect to cellular/genomic equivalents. Sensitivity of detection is expected to be influenced both by this expression level and the tumor purity of the sample. Detection of a particular clinical fusion event for this assay requires that both fusion partners and the specific fusion junction between them be flanked by the amplicon primers used. Adequacy of RNA sampling is ensured by requiring that a sample have a minimum of 500,000 mapped cDNA target reads with a minimum average sequence length of 60 base pairs.

Details and limitations of the test:

- False negative results can be obtained in cases with low fusion RNA expression, low tumor percentage, or fusions that do not correspond exactly to the targeted fusion junctions on the assay. We require a minimum of 20% tumor nuclei in the sample to reduce the potential for false-negative results. Correlation with traditional methods of fusion detection such as fluorescent in situ hybridization (FISH) is recommended as applicable.

Report annotation and generation software: A post-variant calling analysis and annotation tool, OncoSeek version 1.8.1.490, was used in the construction of this report.

DISCLAIMER:

This test was developed and its performance characteristics determined by the Molecular Diagnostic Laboratory (MDL) at the M.D. Anderson Cancer Center. It has not been cleared by the U.S. Food and Drug Administration. However, such approval is not required for clinical implementation, and the test results on the ordered genes have been shown to be

THE UNIVERSITY OF TEXAS
MD Anderson Cancer Center
Making Cancer History®

The University of Texas MD Anderson Cancer Center
1515 Holcombe Blvd., Houston, TX 77030

Print Date: 12/8/2020 10:25 CST
Location: MN Molecular Diag
Ordering: GONZALEZ PA,CIPRIANO C

NAME: XXXXX
MRN: XXXXX
DOB/Age/Sex: X/XX/XXXX 60 years Female

Molecular Diagnostics

clinically useful. This laboratory is CAP accredited and CLIA certified to perform high complexity molecular testing for clinical purposes.

Electronically Signed By: ASIF RASHID, MD - 10160 and reported on 12/08/20 10:25 AM

Test performed by:
The University of Texas MD Anderson Cancer Center Molecular Diagnostic Lab
6565 MD Anderson Blvd
Houston, TX 77030

Supplemental Online Content

Supplementary Methods.

Imaging Mass Cytometry

Imaging mass cytometry was performed at the Flow Cytometry and Cellular Imaging Facility at The University of Texas MD Anderson Cancer Center. A tissue microarray was constructed with 6 representative 1-mm^3 formalin-fixed, paraffin-embedded tissue samples: 2 samples obtained from the primary parotid tumor before the first vaccine dose, 2 samples obtained from pulmonary metastases before the first vaccine dose, and 2 samples obtained from pulmonary metastases after the second vaccine dose.

The tissue microarray was deparaffinized and rehydrated prior to heat-induced antigen retrieval performed by microwaving (MW014-MO, EZ-Retriever system, BioGenex) for 15 minutes at 95 °C in Ph 8.5 EZ-AR 2 (EDTA) buffer (HK522-XAK, BioGenex), blocking with 3% bovine serum albumin plus 1% horse serum in phosphate-buffered saline, and incubation with heavy metal-labelled antibodies specified in Supplementary Table 1 overnight at 4 °C. Slides were washed with TBS-T (TBS plus Tween 0.1%) followed by TBS and then incubated with 0.3125 µM Cell-ID Intercalator-Ir (Cat# 201192A, Fluidigm, 1:400 dilution) for the detection of nuclear DNA.

Metal-conjugated antibodies were detected with a Hyperion Imaging Mass Cytometer (Fluidigm). Tissue was laser ablated at 200 Hz. Data were analyzed by custom image analysis scripts. Cells were first segmented based on DNA signal after band-pass Gaussian filtering using Otsu's method, and overlapping cells were divided by seeded watershed. Intensities for each antibody channel were corrected by lateral compensation as described.[1] Marker combinations used to define cell populations are given in Supplementary Table 2. All analyses were performed in Matlab 2019a (Mathworks).

Tumor Molecular Profiling

Primary tumor molecular profiling was performed using a commercial tumor profiling service (CARIS Molecular Intelligence; CARIS Life Sciences, Texas, USA). Targeted-exome sequencing of the patient's primary tumor was also performed using the Oncomine CDx Target test (Thermo Fisher Scientific).

Supplementary Table 1. Antibodies and Metals Used for Imaging Mass Cytometry

Antibody	Metal	Dilution	Vendor	Catalog No	Antibody Clone
Arginase-1	164DY	50	DVS-Fluidigm	3164027D	D4E3M
B7H4	166Er	100	DVS-Fluidigm	3166030D	H74
CD103	146Nd	50	Cell Signaling Technologies[a]	95835S	EP206
CD11b	149Sm	100	DVS-Fluidigm	3149028D	EPR1344
CD11c	171Yb	100	Abcam	ab216655	EP1347Y
CD16	139La	50	Abcam	ab215977	EPR16784
CD163	147Sm	100	DVS-Fluidigm	3147021D	EDHu-1
CD20	161Dy	50	DVS-Fluidigm	3161029D	H1
CD206	163Dy	150	BIORAD	MCA5552Z	5C11
CD3	170Er	75	DVS-Fluidigm	3170019D	Polyclonal, C-terminal
CD31/PECAM	151Eu	75	DVS-Fluidigm	3151025D	EPR3094
CD4	156Gd	200	DVS-Fluidigm	3156033D	EPR6855
CD45	152Sm	75	DVS-Fluidigm	3152018D	D9M8I
CD45RO	173Yb	100	DVS-Fluidigm	3173016D	UCHL1
CD56	145Nd	50	Cell Marque	156R-94	MRQ-42
CD68	165Ho	100	Thermo Fisher	14068882	KP1
CD8a	162Dy	200	DVS-Fluidigm	3162034D	C8/144B
FOXP3	155Gd	50	DVS-Fluidigm	3155016D	236A/E7
Granzyme B	167Er	50	DVS-Fluidigm	3167021D	EPR20129-217
HLA-DR	174Yb	400	DVS-Fluidigm	3174023D	YE2/36 HLK
iNOS	159Tb	50	Abcam	ab239990	SP126
Ki67	168Er	75	DVS-Fluidigm	3168022D	B56
p63	160Gd	100	Cell Signaling Technologies[a]	13109BF	D2K8X
pan-Keratin	148Nd	100	DVS-Fluidigm	3148020D	C11
PD-L1	172Yb	100	Bethyl Laboratories[a]	BLR020E	BLR020E
Siglec-15	169Tm	100	Thermo Fisher	PA572765	Polyclonal
TIGIT	175Lu	25	Abcam	ab243903	BLR047F
TIM3	154Sm	50	DVS-Fluidigm	3154024D	D5D5R
Vimentin	143Nd	400	DVS-Fluidigm	3143027D	D21H3
α-SMA	141Pr	300	DVS-Fluidigm	3141017D	1A4

[a]Bethyl Laboratories and Cell Signaling Technologies graciously provided antibodies to the MD Anderson Flow Cytometry and Cellular Imaging Facility for use in IMC.

Supplementary Table 2. Cell Populations Analyzed and Corresponding Markers

CD45+ immune Cells	**Markers**
CD8 T cells	CD3+, CD8+
Memory CD8 T cells	CD45RO+ CD8 T cells
CD4 T cells	CD3+, CD4+
Memory CD4 T cells	CD45RO+ CD4 T cells
Regulatory T cells	FoxP3+ CD4 T Cells
All T cells	All CD4 and CD8 T cells
NK cells	CD56+, CD3-
Cytolytic cells	Granzyme B+ and CD56+ or CD8+
B cells	CD20+
Dendritic cells	CD11c+, CD68-
HLA-DR+ dendritic cells	HLA-DR+ dendritic cells
Macrophages	CD68 or CD163+CD206, not T cells, B cells, or dendritic cells
M2 macrophages	CD163+ or CD206+ macrophages
M0/M1 macrophages	Macrophages negative for CD163, CD206, and Arg1
All myeloid cells	All macrophages, dendritic cells, and Arg1+ or CD11b+
Neutrophils	CD16+, not T cells, B cells, or myeloid cells
All immune cells	All immune cells described above
Other cells	
Tumor cells	Pan-cytokeratin+ or p63+, CD31-, non-immune cells
Endothelial cells	CD31+, pan-cytokeratin-, p63-, non-immune cells
Fibroblasts	Vimentin+ or αSMA+, CD31-, pan-cytokeratin-, p63-, non-immune cells
Functional markers	
Proliferating cells	Ki67
T cell function	TIM3, TIGIT

Supplementary Figure 1. Representative hematoxylin and eosin–stained sections.

(A-B) Sections of primary parotid tumor at 4x (A) and 10x (B) magnification. Morphologically, the carcinoma is composed of relatively monotonous round cells with prominent nucleoli and eosinophilic cytoplasm; several areas have a more basophilic and other areas have a rhabdoid/plasmacytic-type appearance of the neoplastic cells. The phenotype is suggestive of a dominant myoepithelial carcinoma. Very rare, scattered mononuclear/lymphocytic elements are noted at the tumor border. (C-D) Section of pre-vaccination lung biopsy specimen at 10x and 4x magnification. The morphology is that of metastatic myoepithelial carcinoma, and entirely resembles the morphology of the primary tumor, including with respect to the immune environment, which has a rare mononuclear/lymphocytic inflammatory infiltrate. (E-F) Sections of post-vaccination lung biopsy specimens at 4x (E) and 10x (F) magnification. There is a massive inflammatory infiltrate with embedded scant tumor clusters (< 5%). The inflammatory infiltrate consists of admixed mononuclear cells (lymphocytes, plasma cells, and monocytes) and a significant number of histiocytes.

A.

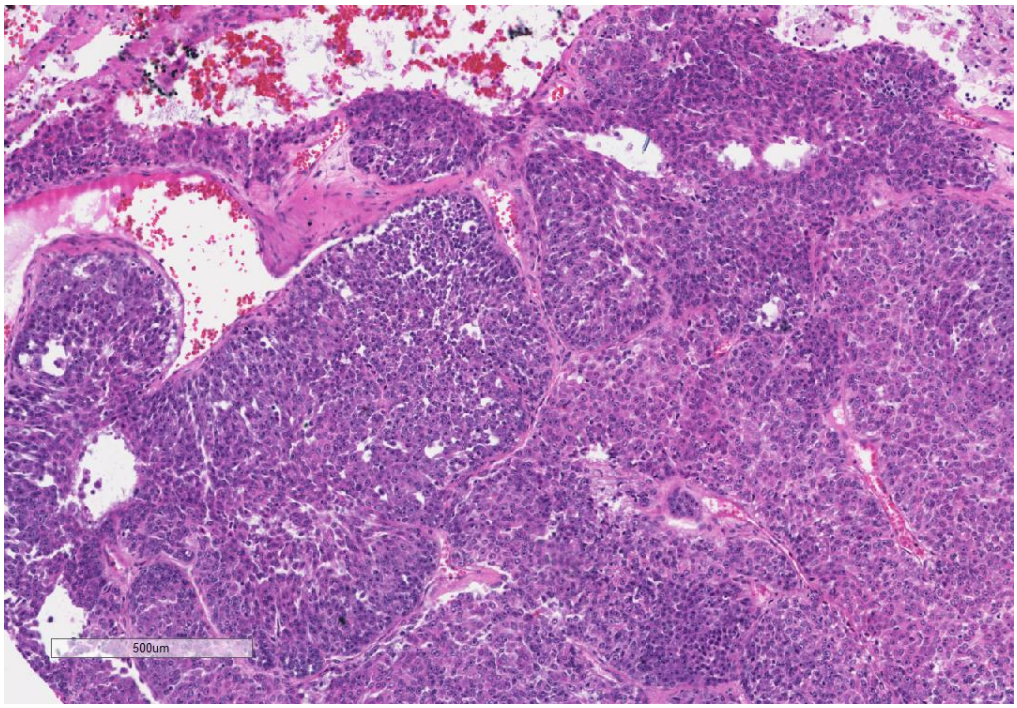

B.

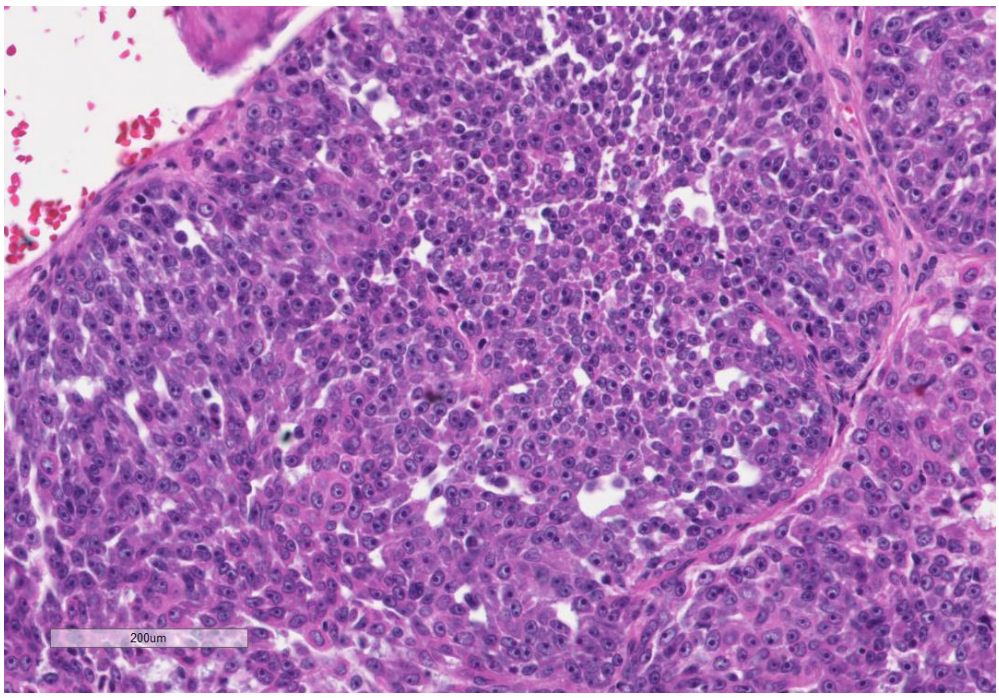

C.

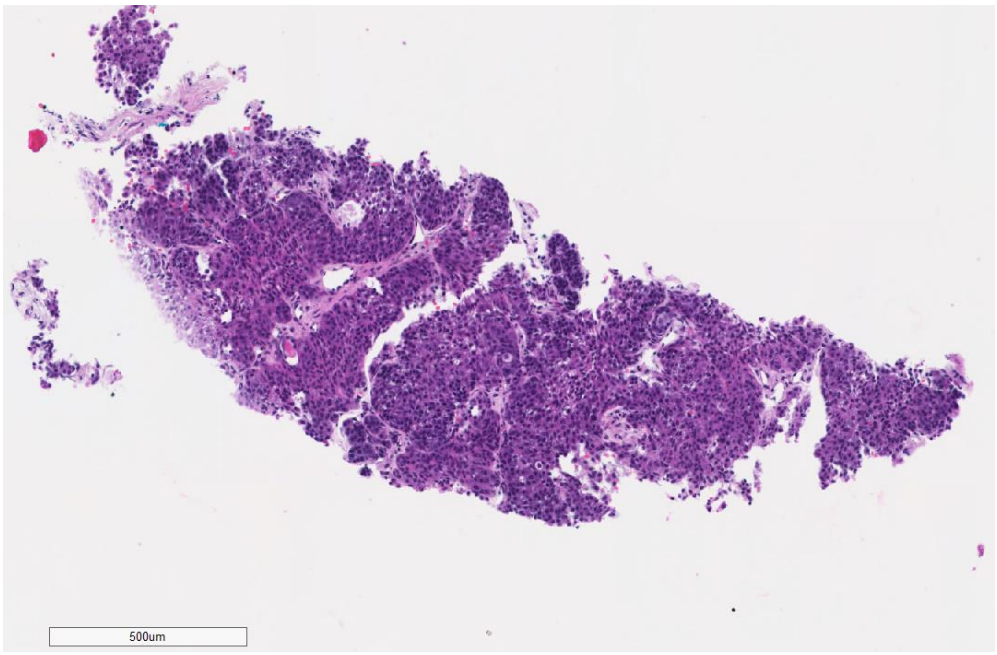

D.

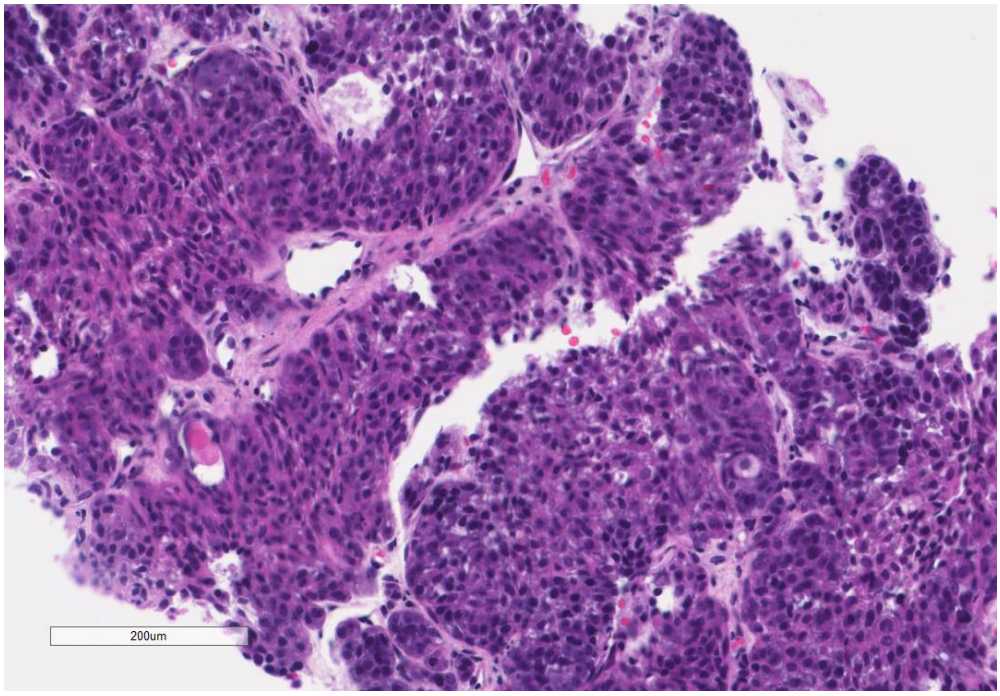

E.

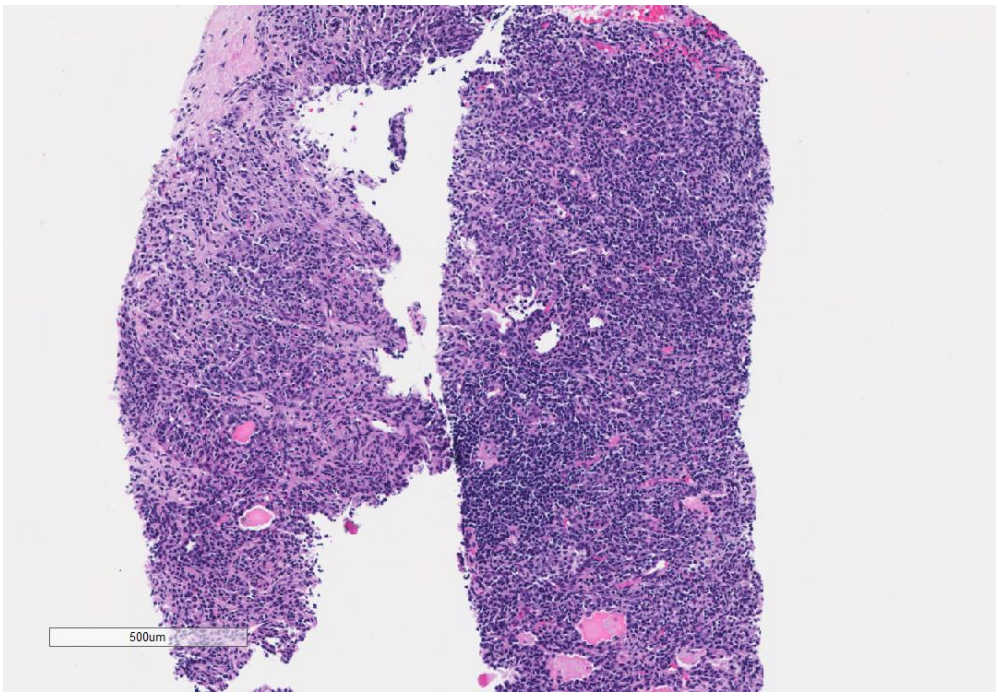

F.

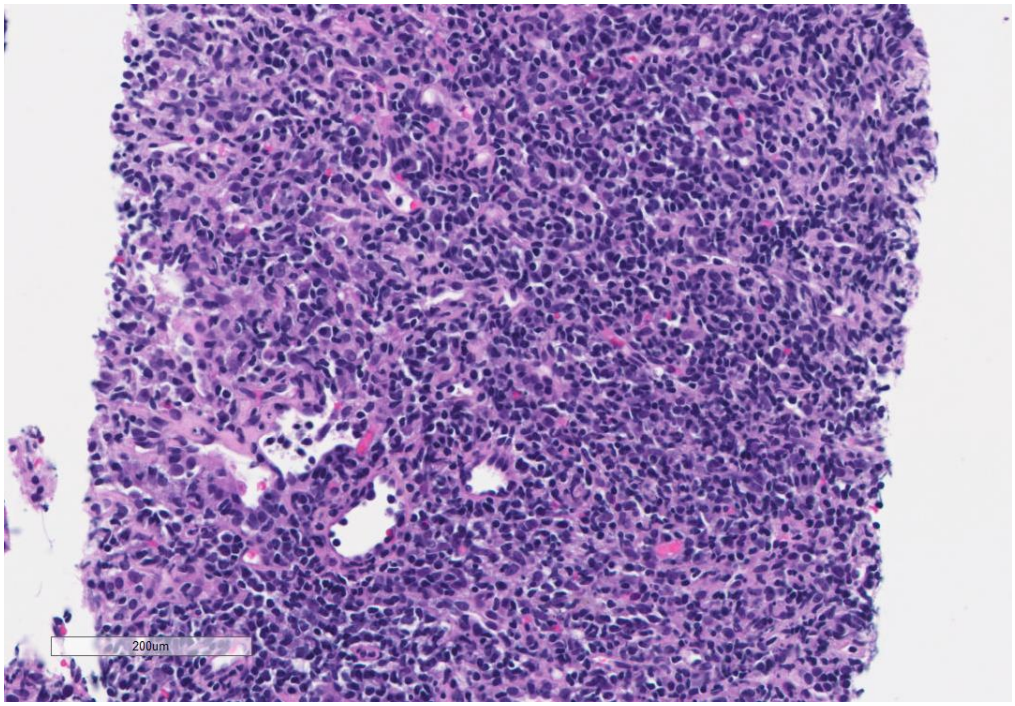

IMAGING MASS CYTOMETRY IMAGES

Supplementary Figure 2. Imaging mass cytometry images showing expression of antibody markers in representative lung biopsy specimens. (A) Pre-vaccine biopsy specimen. All images are of the same region of the same tumor (X, Y 310, 130; height and width, 750 pixels). Scale bars, 100 µm. (B) Post-vaccine biopsy specimen. All images are of the same region of the same tumor (X, Y 5, 85; height and width, 750 pixels). Scale bars, 100 µm.

A.

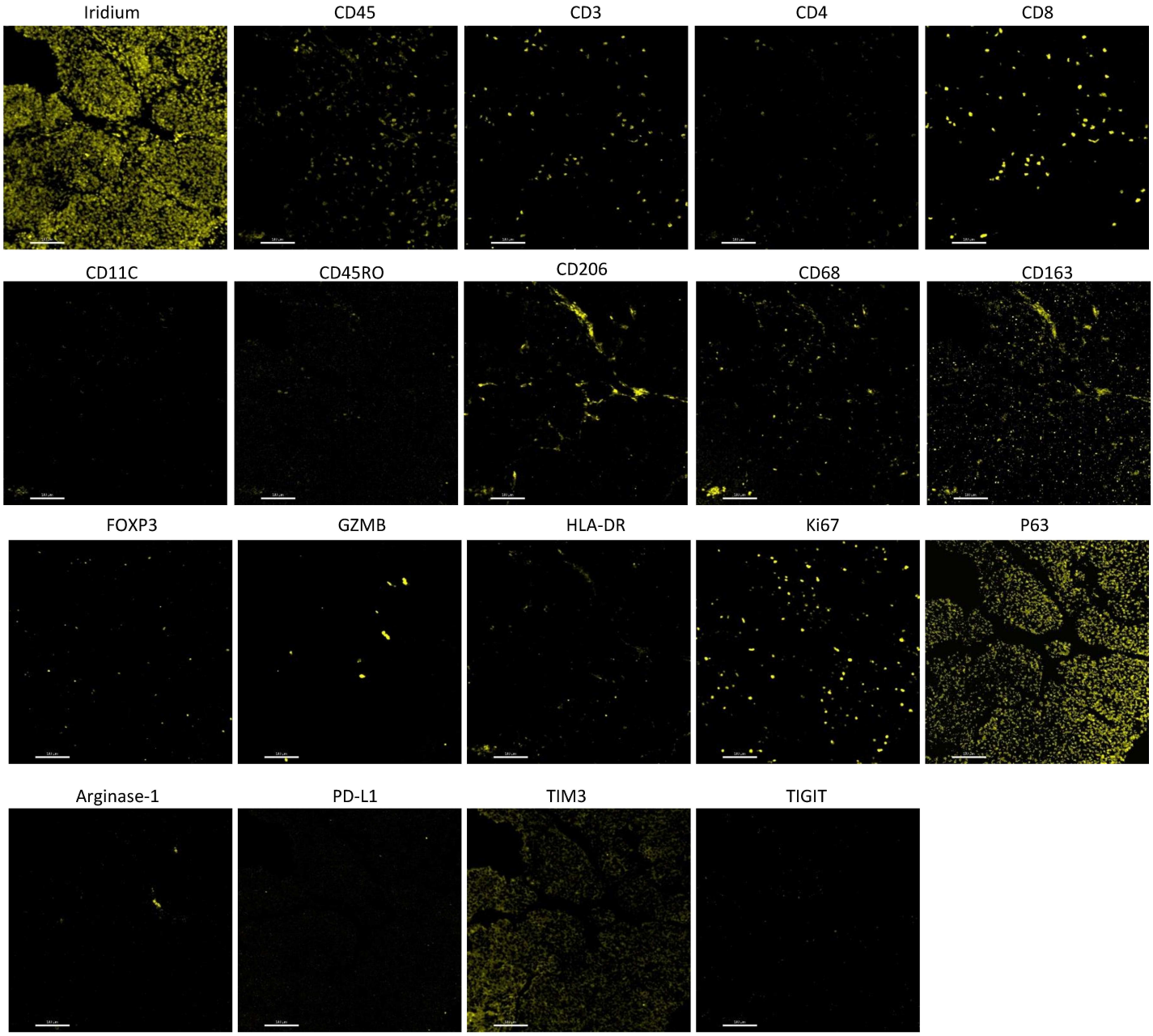

B.

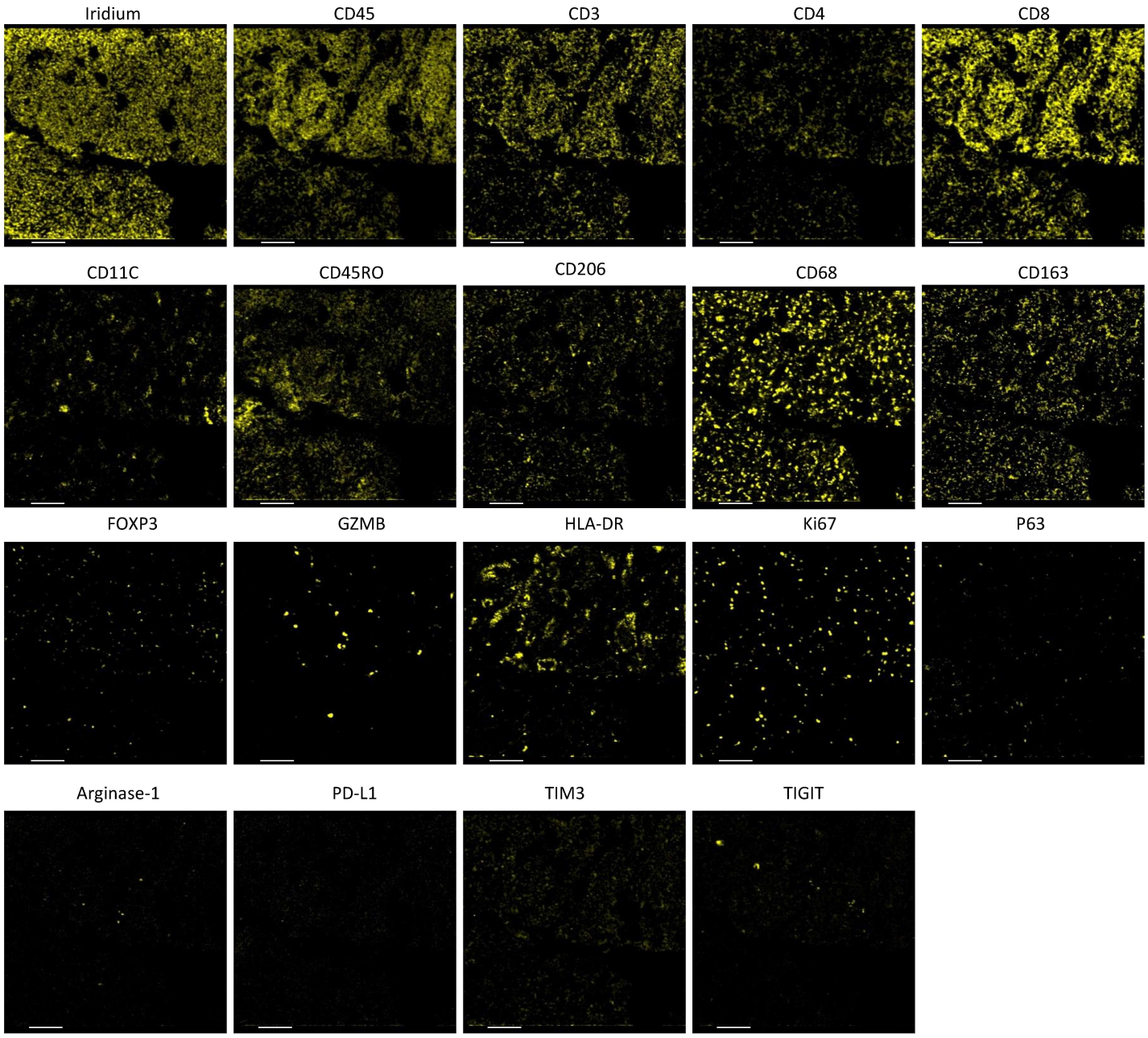
Iridium
CD45
CD3
CD4
CD8
CD11C
CD45RO
CD206
CD68
CD163
FOXP3
GZMB
HLA-DR
Ki67
P63
Arginase-1
PD-L1
TIM3
TIGIT

Reference

1. Bai Y, Zhu B, Rovira-Clave X, et al. Adjacent Cell Marker Lateral Spillover Compensation and Reinforcement for Multiplexed Images. Front Immunol 2021;12:652631.